NEOPLASIA
www.neoplasia.com

Volume 17 Number 10 October 2015 pp. 767–775 767

Identification of Metastasis-Associated Metabolic Profiles of Tumors by ^{1}H-HR-MAS-MRS[1,2,3]

Saurabh S. Gorad*,†, Christine Ellingsen‡, Tone F. Bathen*, Berit S. Mathiesen‡, Siver A. Moestue*,† and Einar K. Rofstad‡

*Department of Circulation and Medical Imaging, Norwegian University of Science and Technology (NTNU), Trondheim, Norway; †St. Olavs University Hospital, Trondheim, Norway; ‡Department of Radiation Biology, Institute for Cancer Research, Oslo University Hospital, Oslo, Norway

Abstract

Tumors develop an abnormal microenvironment during growth, and similar to the metastatic phenotype, the metabolic phenotype of cancer cells is tightly linked to characteristics of the tumor microenvironment (TME). In this study, we explored relationships between metabolic profile, metastatic propensity, and hypoxia in experimental tumors in an attempt to identify metastasis-associated metabolic profiles. Two human melanoma xenograft lines (A-07, R-18) showing different TMEs were used as cancer models. Metabolic profile was assessed by proton high resolution magic angle spinning magnetic resonance spectroscopy (^{1}H-HR-MAS-MRS). Tumor hypoxia was detected in immunostained histological preparations by using pimonidazole as a hypoxia marker. Twenty-four samples from 10 A-07 tumors and 28 samples from 10 R-18 tumors were analyzed. Metastasis was associated with hypoxia in both A-07 and R-18 tumors, and ^{1}H-HR-MAS-MRS discriminated between tissue samples with and tissue samples without hypoxic regions in both models, primarily because hypoxia was associated with high lactate resonance peaks in A-07 tumors and with low lactate resonance peaks in R-18 tumors. Similarly, metastatic and non-metastatic R-18 tumors showed significantly different metabolic profiles, but not metastatic and non-metastatic A-07 tumors, probably because some samples from the metastatic A-07 tumors were derived from tumor regions without hypoxic tissue. This study suggests that ^{1}H-HR-MAS-MRS may be a valuable tool for evaluating the role of hypoxia and lactate in tumor metastasis as well as for identification of metastasis-associated metabolic profiles.

Neoplasia (2015) 17, 767–775

Introduction

Solid tumors are composed of cancer cells and a supporting stroma. The stroma consists of a variety of components, including an extracellular matrix, cancer-associated fibroblasts, immune cells, and blood vessels lined by endothelial cells and a basement membrane [1]. The vascular network of most tumors shows severe morphological and architectural anomalies, resulting in heterogeneous and inadequate blood supply and tissue regions having aberrant physiological conditions characterized by high interstitial fluid pressure (IFP), nutrient deprivation, acidity, and hypoxia [2]. Interactions between the cancer cells, the fibrous and cellular components of the stroma, and the physiological conditions of the tissue result in a tumor microenvironment (TME) that serves as a niche for malignant growth [3].

Address all correspondence to: Einar K. Rofstad, PhD, Department of Radiation Biology, Institute for Cancer Research, Norwegian Radium Hospital, Box 4953 Nydalen, N-0424 Oslo, Norway.
E-mail: einar.k.rofstad@rr-research.no

[1] Financial support was received from the Norwegian Cancer Society, the South-Eastern Norway Regional Health Authority, the Central Norway Regional Health Authority, and the Norwegian University of Science and Technology (NTNU).
[2] The funding sources were not involved in study design; in the collection, analysis, and interpretation of data; in the writing of the report; or in the decision to submit the article for publication.
[3] Conflicts of interest: none
Received 1 July 2015; Revised 25 September 2015; Accepted 5 October 2015

1476-5586
http://dx.doi.org/10.1016/j.neo.2015.10.001

The physiological conditions of the TME deteriorate continuously as tumors evolve, and concurrently, some cancer cells acquire phenotypic traits favoring malignant progression, invasive growth, and metastatic spread [4]. A plethora of genetic determinants of cancer metastasis have been identified, indicating that metastatic cancer cells are genetically equipped to overcome physical barriers, escape from the primary tumor, and survive and grow at secondary sites [5]. Furthermore, it is increasingly recognized that the metastatic process is tightly linked to the oxygenation and acidity of the TME [6]. Hypoxia may facilitate metastasis by inducing genomic instability, by selecting for aggressive cell phenotypes, and by up-regulating the expression of metastasis-promoting genes [7]. Several transcription factors are activated by hypoxia including hypoxia-inducible factor-1 (HIF-1), and targets of HIF-1 play critical roles in many steps of the metastatic process, including cell viability/apoptosis, cell proliferation/growth arrest, tissue remodeling/invasion, and angiogenesis [8]. Low extracellular pH (pH_e) and elevated lactate levels may promote metastasis by both hypoxia-dependent and hypoxia-independent mechanisms [9]. The hypoxia-independent mechanisms include activation of signaling pathways that promote angiogenesis, cell migration, and invasive growth as well as lactate-induced stabilization of HIF-1α under normoxic conditions [10].

Moreover, cancer cells also develop an abnormal metabolic phenotype during tumor evolution, reflecting an increasing need for energy and building blocks for synthesis of macromolecules [11]. In addition, they show metabolic plasticity allowing them to adapt to and thrive under variable and hostile conditions [12,13]. The metabolic abnormalities are directly linked to the genetic drivers of cancer [14]; however, the TME is involved in regulating the metabolism [15]. Similar to the metastatic phenotype, the metabolic phenotype is tightly linked to the oxygenation and acidity of the TME. Hypoxia induces adaptive changes in the metabolism of cancer cells by reprogramming metabolic pathways, an effect that is mediated by HIF-1 [16]. Aerobic and anaerobic glycolysis leads to decreased pH_e and accumulation of lactate, and the metabolic program of cancer cells is altered under acidosis, lactosis, and lactic acidosis [17,18].

Biomarkers for personalized cancer treatment based on the metastatic propensity of the primary tumor are needed. The dynamic nature of cancer cells and the TME makes the identification of such biomarkers highly challenging. However, because of the similarities of the metastatic and metabolic cell phenotypes and their interactions with the TME, we hypothesized that biomarkers of the metastatic propensity of tumors can be detected by metabolic profiling. Metabolic profiles of tumors provide a snap-shot of their metabolic status at biopsy, reflecting the overall activity of both the cancer and stromal cells [19].

In this study, we searched for relationships between metabolic profile and metastatic propensity in two melanoma xenograft models (A-07, R-18). Approximately 50% of the tumors of these models give rise to lymph node (A-07, R-18) and/or pulmonary (A-07) metastases [20,21]. Metabolic profiles of the primary tumors of mice with and mice without metastases were obtained by proton high resolution magic angle spinning magnetic resonance spectroscopy (^{1}H-HR-MAS-MRS). Hypoxic regions within the tumors and tissue samples analyzed by ^{1}H-HR-MAS-MRS were detected by immunohistochemistry, using pimonidazole as a hypoxia marker. The primary aim of the study was to provide novel insight into associations between metabolism, metastatic propensity, and hypoxia in tumors in an attempt to identify metastasis-associated metabolic profiles.

Materials and Methods

Mice

Adult (8-10 weeks of age) female BALB/c *nu/nu* mice weighing 25 to 28 g were used as host animals for tumors. The mice were bred at our institute and were maintained under specific pathogen-free conditions at constant temperature (24-26°C), constant humidity (30%-50%), and a 12-hour light/12-hour dark cycle. Sterilized food and tap water were given *ad libitum*. The animal experiments were approved by the institutional committee on research animal care and were done according to the U.S. Public Health Service Policy on Humane Care and Use of Laboratory Animals.

Tumor Models

The A-07 and R-18 human melanoma cell lines were established as described earlier [22]. The cells used in the present experiments were obtained from our frozen stock and were maintained in monolayer culture in RPMI 1640 (25 mmol/l HEPES and L-glutamine) supplemented with 13% bovine calf serum, 250 mg/l penicillin, and 50 mg/l streptomycin. Xenografted tumors were initiated by inoculating aliquots of ~3.5×10^5 cells intradermally into the left mouse flank. Tumor volume (V) was calculated as $V = \pi/6 \times a \times b^2$, where a is the longer and b is the shorter of two perpendicular tumor diameters, measured with callipers [22]. Experiments were carried out when the tumors had grown to a volume of 200–300 mm^3. The tumors were snap-frozen in liquid nitrogen immediately after resection and stored at −80°C until analysis.

Tumor Hypoxia

Pimonidazole [1-[(2-hydroxy-3-piperidinyl)-propyl]-2-nitroimidazole] was administered intraperitoneally in doses of 30 mg/kg and used as a marker of tumor hypoxia [23]. Tumors were resected ~4 h after the pimonidazole administration, and histological sections were prepared by using standard procedures. Immunohistochemistry was performed by using an avidin–biotin peroxidase-based staining method [24]. An anti-pimonidazole rabbit polyclonal antibody (gift from Professor Raleigh, Department of Radiation Oncology, University of North Carolina School of Medicine, Chapel Hill, NC) was used as primary antibody. Diaminobenzidine was used as chromogen, and hematoxylin was used for counterstaining. Three or four sections were examined for each tumor sample.

Metastases

Lymph node and pulmonary metastases were detected as described elsewhere [25,26]. Briefly, after the mice had been euthanized and the primary tumor and the lungs had been resected, the mouse bodies were examined for external lymph node metastases in the inguinal, axillary, interscapular, and submandibular regions and internal lymph node metastases in the abdomen and mediastinum. The presence of metastatic growth in enlarged lymph nodes was confirmed by histological examination. Microscopic pulmonary metastases were detected by histological analysis of the resected lungs. Histological sections were cut at 100-μm intervals throughout the entire lobes and stained with hematoxylin and eosin. Groups of five or more tumor cells were scored as a metastasis.

^{1}H-HR-MAS-MRS

^{1}H-HR-MAS-MRS was carried out at the MR Core Facility at NTNU, Trondheim, Norway, on a 14.1-T Bruker Avance DRX600 spectrometer equipped with a ^{1}H/^{13}C dual nuclei probe (Bruker

BioSpin GmbH, Ettlingen, Germany). Frozen tumor tissue samples were cut to an appropriate size (mean weight: 8.32 mg, weight range: 3.0–16.2 mg) and placed in 30-µl disposable rotor inserts filled with 3 µl of a cooled solution of 24.29-mM sodium formate (chemical shift reference) in D_2O. A dedicated work station bench cooled with liquid nitrogen was used to keep the samples frozen [27]. Inserts with frozen samples were transferred to the 4-mm diameter zirconium rotors of the spectrometer, and spectra were acquired at a 5-kHz spin rate and an instrument temperature of 5°C. Spin-echo spectra were recorded by using a Carr-Purcell-Meiboom-Gill (CPMG) pulse sequence (Bruker: cpmgprld) with 4-second water suppression prior to a 90° excitation pulse. T_2 filtering was obtained by using an inter-echo spacing of 0.6 ms, resulting in an effective TE of 77 ms. A total of 256 scans over a spectral region of 12 kHz were collected into 72 K points with an acquisition time of 3.06 s. A standard 0.4-mM creatine reference solution was analyzed under identical experimental conditions and used as an external calibration standard.

Preprocessing and Quantification of Metabolites

Preprocessing of CPMG spectra was performed by using TopSpin 3.1 (Bruker). The raw data were multiplied by a 0.30-Hz exponential weighting function and Fourier transformed. The automatic phase and baseline correction routine was applied to each spectrum. The chemical shifts were calibrated to the lactate peak at 1.33 ppm, and peak assignments were performed according to the human metabolome database and previously published data [28]. The peak areas of lactate (1.33 ppm), creatine (3.03 ppm), choline (3.19 ppm), phosphocholine (PCho; 3.21 ppm), glycerophosphocholine (GPC; 3.22 ppm), taurine (3.42 ppm), and glycine (3.56 ppm) were determined by fitting Voigt curves to the data by polynomial regression (PeakFit v 4.12; Systat Software Inc, Chicago, IL, USA). The correlation coefficients of the fits were ≥0.95 for all spectra. The concentrations of the individual metabolites were calculated with reference to the peak area of the standard creatine solution according to the PULCON (pulse length based concentration determination) principle [29] and normalized to the sample weight.

Multivariate Analysis

Multivariate analysis was carried out by using the spectral region between 0.63 and 4.73 ppm, which contained the majority of the metabolite information. The spectra were shift-referenced to creatine, baseline corrected, and normalized to equal total areas. Peak alignment was done by using the icoshift algorithm of MATLAB 7.14.0.739 [30]. Partial least square discriminant analysis (PLS-DA) was carried out to explore relationships between metabolic profile, tumor hypoxia, and metastasis. Hence, the following comparisons of metabolic profiles were made: A-07 tumors versus R-18 tumors, hypoxic versus non-hypoxic tumors (A-07 and R-18), metastatic versus non-metastatic tumors (lymph node metastases, A-07 and R-18; pulmonary metastasis, A-07). The PLS-DA models were validated by leave-one-out cross-validation, where all spectra from one tumor were either kept in the training data or used to test the model. The number of latent variables (LVs) giving first minimum classification error was chosen. Validation of the classification results was done by permutation testing (n = 1000, significance for $P < .05$), where the class labels were shuffled to resemble random classification. The multivariate analysis was carried out in MATLAB R2012a using PLS_toolbox 6.2.1 (Eigenvector Research, Inc., Wenatchee, WA).

Statistical Analysis of Metabolite Concentrations

An unpaired Student's *t*-test was performed to detect significant differences in metabolite concentrations between hypoxic and non-hypoxic tissue samples and between metastatic and non-metastatic tumors. The threshold for statistical significance was defined as $P \leq .05$.

Results

Hypoxia and Metastasis Characteristics of the Tumors Analyzed by ^{1}H-HR-MAS-MRS

Twenty-four samples from 10 A-07 tumors and 28 samples from 10 R-18 tumors (two or three samples from each tumor) were subjected to ^{1}H-HR-MAS-MRS. The hypoxia and metastasis data of the tumors and samples are summarized in Table 1. Metastasis was associated with hypoxia in both tumor models. For the A-07 model, hypoxic tissue was detected in three of the five tumors that developed lymph node metastases, in one of the five tumors that did not develop lymph node metastases, in four of the four tumors that developed pulmonary metastases, and in none of the six tumors that did not develop pulmonary metastases. For the R-18 model, four of the four metastatic tumors and two of the six non-metastatic tumors showed regions with positive hypoxia staining.

The A-07 and R-18 Tumor Models Showed Distinctly Different Metabolic Profiles

^{1}H-HR-MAS-MRS revealed that the metabolic profiles of the A-07 and R-18 models were significantly different. Visual inspection of the mean spectra suggested lower PCho, GPC, glycine, and creatine levels and higher lactate levels in the A-07 tumors than in the R-18 tumors (Figure 1*A*). PLS-DA, taking into account the entire metabolic profiles (i.e., all detectable metabolites including taurine, alanine, glutamate, glutamine, glycerol, and glucose), discriminated clearly between the two tumor models (Table 2). The score plot showed that the A-07 samples were clustered on the right side of the plot with high LV1 scores, while the R-18 samples were clustered on the left side with low LV1 scores (Figure 1*B*). Consistent with the mean spectra, the loading profile showed that the A-07 samples were characterized by high levels of lactate and low levels of PCho, GPC, glycine, and creatine compared with the R-18 samples (Figure 1*C*). These observations were in agreement with the quantification data (Supplementary Table S1), with the exception that the lactate levels were not significantly different in univariate analysis. The other metabolites generally showed low intensity in the loading profile, suggesting that their contribution to the discrimination was low.

^{1}H-HR-MAS-MRS of A-07 Tumors Revealed Metabolic Differences between Hypoxic and Non-Hypoxic Tissue Samples, but not between Metastatic and Non-Metastatic Tumors

For the A-07 model, PLS-DA revealed significant differences between the metabolic profiles of the samples with and the samples without hypoxic tissue (Table 2). The two groups of samples were clearly separated in the 3D score plot (Figure 2*A*), primarily because the lactate levels were higher and the GPC levels were lower in the hypoxic samples than in the non-hypoxic samples, as shown in the 3D loading plot (Figure 2*B*). Even though the tumors that developed pulmonary metastases were the same as those that showed positive hypoxia staining, PLS-DA did not discriminate between the tumors that metastasized to the lungs and those that did not (Table 2), most likely because three of the 11 samples from the metastasis-positive

Table 1. Characteristics of the Tumor Tissue Analyzed by ^{1}H-HR-MAS-MRS

	A-07 Tumors (n = 10)		A-07 Samples (n = 24)		R-18 Tumors (n = 10)		R-18 Samples (n = 28)	
	Positive (n)	Negative (n)	Positive (n)	Negative (n)	Positive (n)	Negative (n)	Positive (n)	Negative (n)
Hypoxia	4	6	8	16	6	4	14	14
Lymph node metastasis	5	5	13	11	4	6	12	16
Lung metastasis	4	6	11	13	-	-	-	-

n, number of replicates = the number used for multivariate analysis and quantification of metabolites.

tumors did not show positive staining for hypoxia and thus did not contain detectable hypoxic regions (Table 1). The 3D score plot and 3D loading plot are shown in Figure 2, *C* and *D*. Significant differences between the metabolic profiles of the tumors in lymph node positive and lymph node negative mice were not detected either (Table 2; Figure 2, *E* and *F*), probably because five of the 13 samples from the metastatic tumors did not have detectable regions with hypoxic tissue (Table 1). Moreover, univariate analyses of metabolite concentrations did not reveal significant differences between the hypoxic and non-hypoxic samples or between the metastatic and non-metastatic tumors, with the only exception that the creatine concentration was lower in the tumors that developed pulmonary metastases than in those that did not (P = .03, Supplementary Table S1).

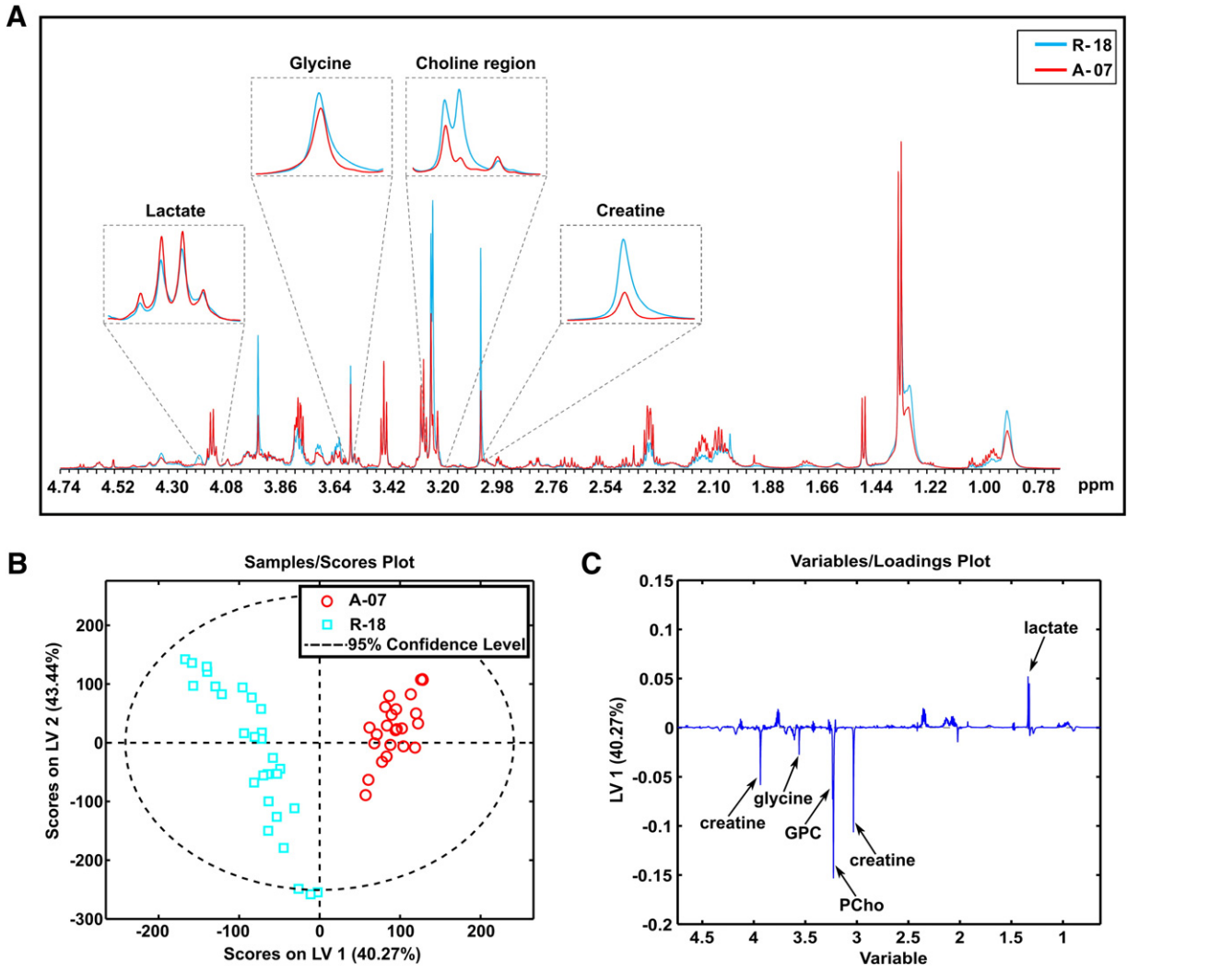

Figure 1. Metabolic profiles of A-07 and R-18 tumors. Mean ^{1}H-HR-MAS-MR spectra (A), PLS-DA score plot (B), and loading plot (C) of tissue samples from A-07 and R-18 tumors. The samples from the A-07 tumors were clearly separated from those from the R-18 tumors. The A-07 tumors showed higher levels of lactate and lower levels of PCho, GPC, glycine, and creatine than the R-18 tumors. PLS-DA classification accuracy: 100%.

Table 2. PLS-DA Classification of the A-07 and R-18 Tumor Models Based on Metabolic Profile, Tissue Hypoxia, and Metastasis

Input	LVs	Classification accuracy (%)	Sensitivity (%)	Specificity (%)	*P*
A-07 vs R-18	2	100	100	100	<.001
A-07 (hypoxic vs non-hypoxic)	3	71	62.5	81.3	.033
A-07 (lung metastasis positive vs lung metastasis negative)	3	57.3	45.5	69.2	.282
A-07 (lymph node metastasis positive vs lymph node metastasis negative)	3	50	54.5	46.2	.403
R-18 (hypoxic vs non-hypoxic)	3	85.7	78.6	92.9	.001
R-18 (lymph node metastasis positive vs lymph node metastasis negative)	3	92.7	91.7	93.8	<.001

Classification accuracy, sensitivity, and specificity were determined by leave-one-out cross-validation. *P* values were based on 1000 permutations.

^{1}H-HR-MAS-MRS of R-18 Tumors Revealed Metabolic Differences between Hypoxic and Non-Hypoxic Tissue Samples as well as between Metastatic and Non-Metastatic Tumors

For the R-18 model, PLS-DA differentiated significantly between the metabolic profiles of the samples with and the samples without hypoxic regions as well as between the tumors of mice with and the tumors of mice without lymph node metastases (Table 2). The 3D score plot clearly separated the hypoxic samples from the non-hypoxic samples (Figure 3*A*), and the 3D loading plot revealed that the separation arose mainly because the hypoxic samples showed higher levels of PCho and creatine and lower levels of lactate than the non-hypoxic samples (Figure 3*B*). Similarly, the metastatic tumors were clearly separated from the non-metastatic ones (Figure 3*C*), primarily because the metastatic tumors showed higher levels of PCho, creatine, and glycine and lower levels of lactate than the non-metastatic tumors (Figure 3*D*). The quantitative metabolite analyses showed that the concentration of lactate was higher in the non-hypoxic samples than in the hypoxic samples ($P = .05$) and higher in the non-metastatic tumors than in the metastatic tumors ($P = .03$), whereas the concentration of the other metabolites did not differ significantly between the hypoxic and non-hypoxic samples or between the metastatic and non-metastatic tumors (Supplementary Table S1).

Discussion

The metastatic spread of malignant cells from the primary tumor to distant organ sites such as lymph nodes, lungs, and brain is a major cause of death in cancer patients. Hypoxia, low pH_e, and elevated lactate concentration in the TME have been shown to promote metastatic dissemination by several mechanisms [6–10,17,31]. In the present investigation, we searched for relationships between the metabolic profile of tumors as assessed by ^{1}H-HR-MAS-MRS, their hypoxia status, and their metastatic propensity. A-07 and R-18 melanoma xenografts with volumes of 200–300 mm^3 were used as preclinical models of human cancer. These models show highly different TMEs, and approximately 50% of the tumors of both models have developed hypoxic regions and/or distant metastases at this size [20–22]. Furthermore, 200–300-mm^3 A-07 and R-18 tumors do not have necrotic regions [22], and consequently, they should be excellent models for providing novel information on the questions addressed in the study reported herein.

Previous studies have shown that A-07 tumors differ from R-18 tumors in several cellular and microenvironmental properties, including growth rate, metastatic pattern, angiogenic potential, microvascular density (MVD), fraction of hypoxic tissue, IFP, cell density, and extravascular extracellular volume fraction [20–23,32–34]. This study showed that A-07 tumors differ markedly from R-18 tumors also in metabolic profile. The metabolic quantification data revealed that the difference was mainly a consequence of lower levels of PCho, GPC, glycine, and creatine in the A-07 tumors than in the R-18 tumors. Several studies have provided evidence that the metabolism of choline in cancer cells is regulated by aberrantly activated oncogenic signaling pathways [35,36]. High levels of choline-containing compounds have been linked to malignant transformation and high rates of cell proliferation [35–38]. A-07 tumors show significantly higher rates of cell proliferation and volumetric growth than R-18 tumors [22], suggesting that high levels of choline-containing compounds are not associated with high tumor growth rate. The higher levels of PCho, GPC, glycine, and creatine in R-18 tumors than in A-07 tumors may reflect the difference in cell density, since R-18 tumors have approximately two-fold higher cell density and correspondingly lower extravascular extracellular volume fraction than A-07 tumors [33].

A-07 tumors may metastasize to the lungs as well as to external and/or internal lymph nodes of the host mice [20]. Previous studies have revealed that metastatic spread in A-07 tumors is associated with several features of the TME, including high IFP in the tumor center, high MVD in the tumor periphery, and high fraction of hypoxic tissue [20,24,39–41]. Hypoxia in central tumor regions has been identified as the principal driver of the metastatic process in this tumor model, and it has been shown that acute fluctuating hypoxia promotes metastasis to a greater extent than chronic hypoxia [24,39,40]. By exposing tumor-bearing mice to acute fluctuating hypoxia *in vivo*, we have shown that hypoxia promotes metastasis in A-07 tumors primarily by up-regulating the expression of vascular endothelial growth factor-A [41]. The present study confirmed that lung and lymph node metastasis is associated with hypoxia in A-07 tumors. Moreover, it showed that the metabolic profile differed between tumor samples that contained hypoxic tissue and tumor samples that did not stain positive for hypoxia. PLS-DA revealed that the GPC levels were lower and the lactate levels were higher in the hypoxic samples than in the non-hypoxic samples. On the other hand, PLS-DA did not discriminate between the samples from the metastatic and non-metastatic tumors, even though the tumors that gave rise to lung metastases were the same as those that contained hypoxic tissue. The fraction of hypoxic tissue in 200–300-mm^3 A-07 tumors is low, usually less than 10% [23], and consequently, some samples from the metastatic tumors did not stain positive for pimonidazole. The inability of ^{1}H-HR-MAS-MRS to discriminate between metastatic and non-metastatic A-07 tumors most likely resulted from the fact that some samples from the metastatic tumors were derived from non-hypoxic tumor regions.

R-18 tumors may develop lymph node metastases, but do not metastasize to the lungs [21]. Previous studies have revealed that tumor hypoxia is the principal driver of metastasis also in this model [21,24,40,42,43]. Moreover, we have provided significant evidence that hypoxia promotes metastasis in R-18 tumors by up-regulating the urokinase-type plasminogen activator receptor [21,42]. Consistent with our previous studies, lymph node metastasis was associated with hypoxia in the primary tumor also in this study. ^{1}H-HR-MAS-MRS discriminated between metastatic and non-metastatic tumors as well as between hypoxic and non-hypoxic samples, and the score and loading plots for metastatic status were similar to those for hypoxia status. A common feature of the

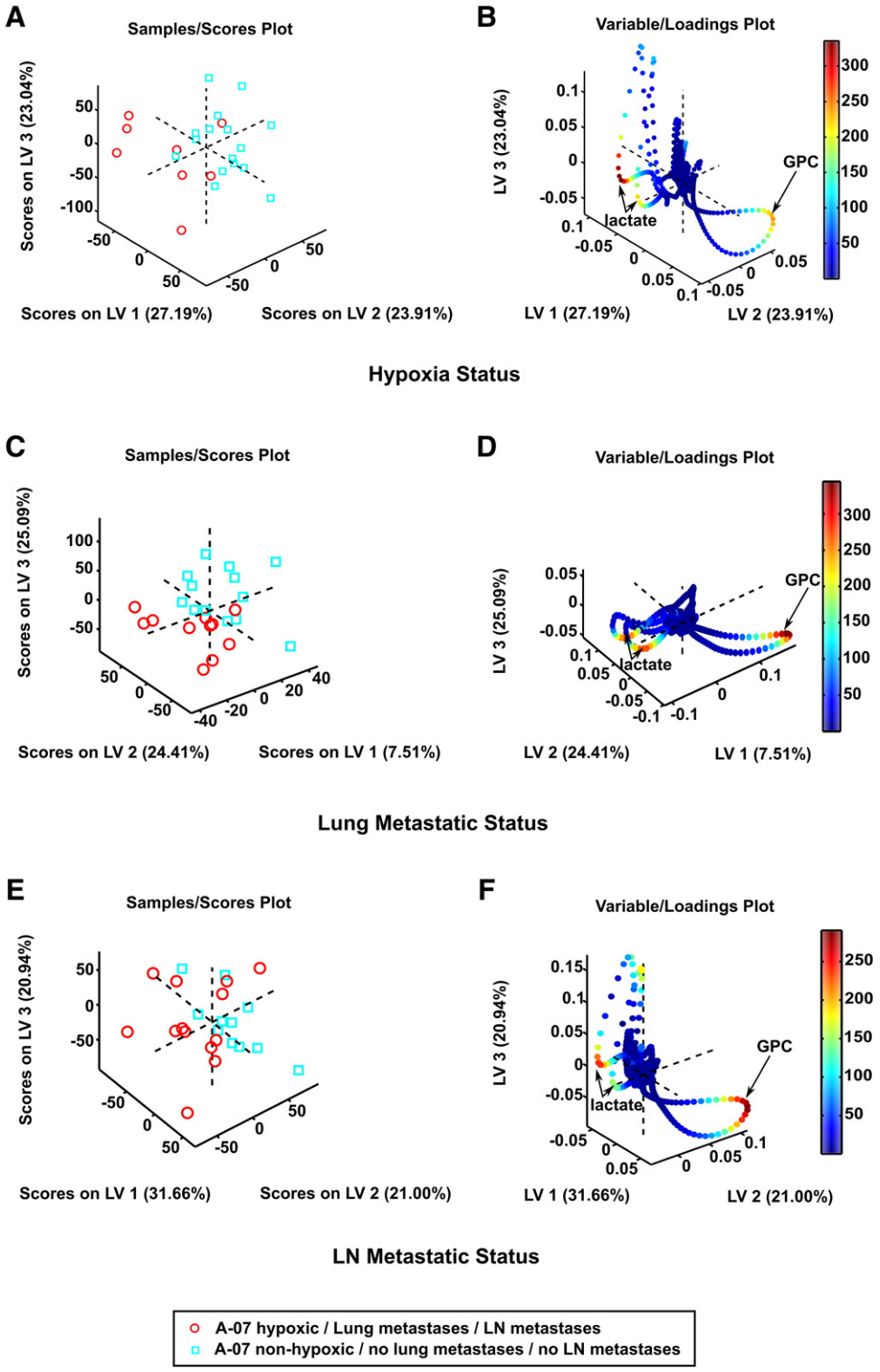

Figure 2. Metabolic profiles of A-07 tissue samples. 3D PLS-DA score plot (A) and corresponding loading plot (B) of samples with and samples without hypoxic regions, 3D PLS-DA score plot (C) and corresponding loading plot (D) of samples from tumors that did and samples from tumors that did not develop lung metastases, and 3D PLS-DA score plot (E) and corresponding loading plot (F) of samples from tumors that did and samples from tumors that did not develop lymph node metastases. The loadings are colored according to their Variable Importance in Projection (VIP) scores. The samples containing hypoxic tissue were clearly separated from the non-hypoxic samples [PLS-DA classification accuracy: 71% (sensitivity: 62.5%; specificity: 81.3%)], whereas the samples from the tumors that developed lung metastases were not separated from the samples from the tumors that did not develop lung metastases, and the samples from the tumors that developed lymph node metastases were not separated from the samples from the tumors that did not develop lymph node metastases.

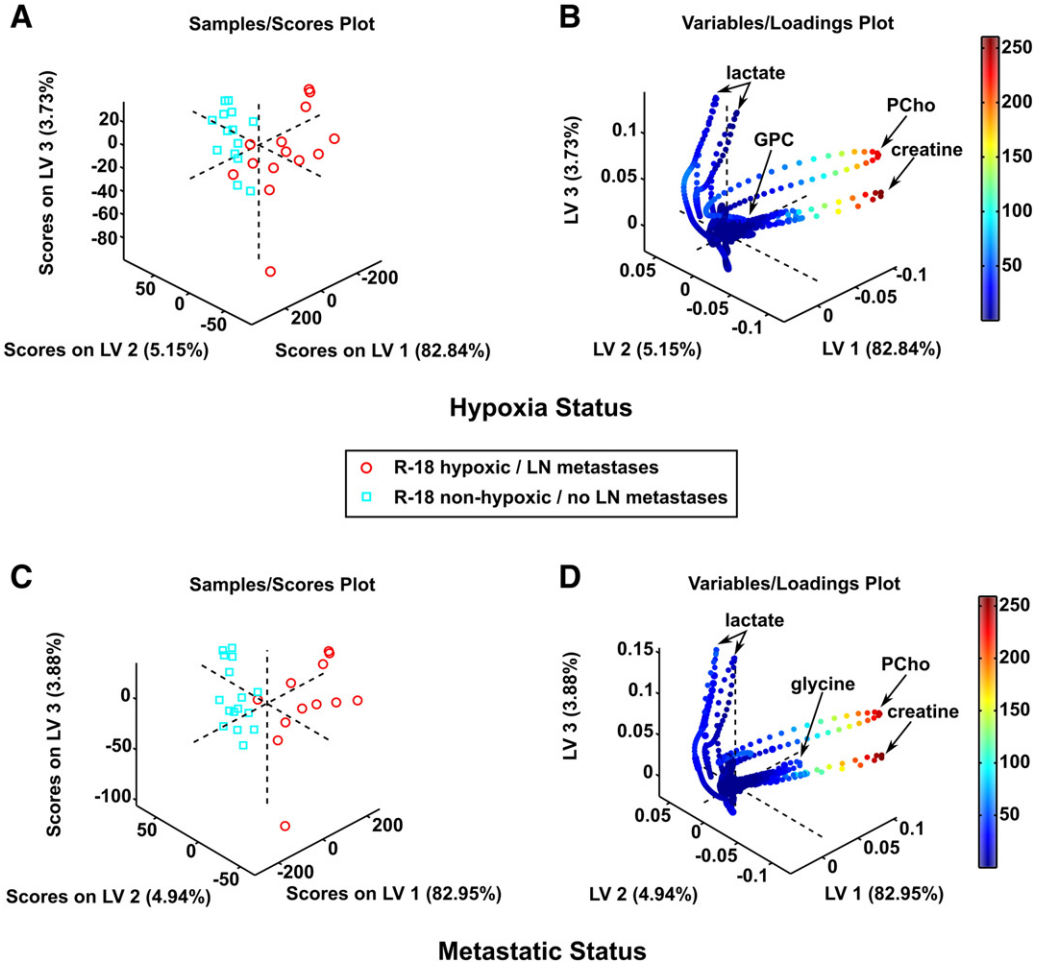

Figure 3. Metabolic profiles of R-18 tissue samples. 3D PLS-DA score plot (A) and corresponding loading plot (B) of samples with and samples without hypoxic regions, and 3D PLS-DA score plot (C) and corresponding loading plot (D) of samples from metastatic and samples from non-metastatic tumors. The loadings are colored according to their VIP scores. The samples containing hypoxic tissue were clearly separated from the non-hypoxic samples [PLS-DA classification accuracy: 85.7% (sensitivity: 78.6%; specificity: 92.9%)] and the samples from the metastatic tumors were clearly separated from those from the non-metastatic tumors [PLS-DA classification accuracy: 92.7% (sensitivity: 91.7%; specificity: 93.8%)].

metastatic tumors and the hypoxic samples was that they had higher levels of PCho and creatine and lower levels of lactate than their non-metastatic and non-hypoxic counterparts, as revealed by the PLS-DA. Choline kinase, the enzyme converting choline to PCho, is up-regulated under hypoxic conditions, and this up-regulation is considered to be an adaptive response contributing to cell survival in a hypoxic TME [44]. Our findings are also consistent with a recent study of the B16F10 murine melanoma line, which suggested that alterations in creatine and choline metabolism are associated with invasive growth and the development of lung and liver metastases [45].

The present study provides increased insight into the relationship between metastasis, hypoxia, and lactate concentration in tumors. Pulmonary and lymph node metastasis was associated with hypoxia in A-07 tumors, and lymph node metastasis was associated with hypoxia in R-18 tumors. The ^{1}H-HR-MAS-MRS analysis showed that hypoxia was associated with high lactate level in A-07 tumors and that both hypoxia and lymph node metastasis were associated with low lactate level in R-18 tumors. Clinical studies involving carcinoma of the uterine cervix, head and neck carcinoma, and rectal adenocarcinoma have suggested that poor survival rates and high incidence of metastases are associated with high hypoxic fraction [46–48] as well as high lactate concentration [49–51]. The A-07 data reported herein are consistent with these clinical observations, but not the R-18 data.

Tumor cells produce lactate from glucose by aerobic as well as anaerobic glycolysis, and they generally show increased glucose consumption under hypoxic conditions [2,17]. However, there is some evidence that the lactate level in tumors is not merely a reflection of the extent of hypoxia [10]. Several preclinical studies have searched for associations between lactate concentration and hypoxia by comparing different tumor lines, individual tumors of the same line, and subregions of single tumors, and some studies showed significant associations whereas others did not [52–56]. Generally, the lactate level was found to be unrelated to the extent of hypoxia in tumors showing increased glycolytic flux [9,10].

The concentration of lactate in tumors is determined by the rate of glycolysis and the rate of clearance by the microvasculature [2,9]. Studies of cells in culture have shown that the rate of aerobic glycolysis is lower in R-18 cells than in A-07 cells, and in contrast to A-07 cells, R-18 cells do not show increased rates of glucose uptake and lactate release under hypoxia [Rofstad, unpublished data]. Even though R-18 tumors have

high fractions of hypoxic tissue, the microvasculature of the tumors may remove lactate efficiently from hypoxic tissue regions. The majority of the hypoxic cells in R-18 tumors are acutely hypoxic caused by high-frequency fluctuations in blood flow, and furthermore, the hypoxic regions in R-18 tumors show high density of plasma channels and extremely narrow vessels devoid of red blood cells [57].

Although there is strong evidence from clinical studies that metastasis is associated with high lactate concentration in the primary tumor [10], a recent review questioned the suggestion that this is a universal feature of malignant diseases in humans [58]. Moreover, some preclinical studies of breast cancer have concluded that the lactate level in tumors does not appear to be correlated with tumor metastatic potential [59,60]. Interestingly, the R-18 data reported herein are similar to those of Xu et al. [60], who used hyperpolarized ^{13}C-pyruvate MRS to study the metabolism of breast carcinoma xenografts and found that the less metastatic tumors produced more lactate than the highly metastatic ones.

In summary, A-07 and R-18 tumors show highly different cellular and microenvironmental properties, and ^{1}H-HR-MAS-MRS discriminated between tumor samples with and without hypoxic tissue in both tumor models. In many hypoxic A-07 samples, the hypoxic regions constituted less than 10% of the samples, suggesting that ^{1}H-HR-MAS-MRS has high power to discriminate between hypoxic and non-hypoxic tumors. However, the discrimination power may be limited to tumors showing significant associations between hypoxia and the concentration of lactate and/or choline-containing compounds. Moreover, TME-associated metastasis is driven by hypoxia in both A-07 and R-18 tumors [21,24,39,40,42,43], and ^{1}H-HR-MAS-MRS discriminated between the R-18 tumors that gave rise to lymph node metastases and those that did not at a high classification accuracy. On the other hand, ^{1}H-HR-MAS-MRS did not discriminate between metastatic and non-metastatic A-07 tumors, most likely because some of the samples from the metastatic tumors were derived from non-hypoxic tumor regions. This reflects a weakness of the ^{1}H-HR-MAS-MRS method that it shares with other biopsy-based methods for characterizing heterogeneous malignant tumors. Taken together, our observations support the notion that metastasis-associated metabolic profiles may be identified by ^{1}H-HR-MAS-MRS and suggest that ^{1}H-HR-MAS-MRS-assessed metabolic profiles may be useful for evaluating the role of hypoxia and lactate in tumor metastasis. Further studies of the association between TME-induced metastasis and metabolic profile may provide new insights into metastatic mechanisms and lead to identification of prognostic biomarkers for use in clinical risk assessment.

Supplementary data to this article can be found online at http://dx.doi.org/10.1016/j.neo.2015.10.001.

Acknowledgments

The authors thank the staff at the MR Core Facility, NTNU, Trondheim and the staff at the Department of Comparative Medicine, OUS, Oslo, Norway, for technical assistance.

References

[1] Mueller MM and Fusenig NE (2004). Friends or foes—bipolar effects of the tumor stroma in cancer. *Nat Rev Cancer* **4**, 839–849.

[2] Vaupel P, Kallinowski F, and Okunieff P (1989). Blood flow, oxygen and nutrient supply, and metabolic microenvironment of human tumors: a review. *Cancer Res* **49**, 6449–6465.

[3] Quail DF and Joyce JA (2013). Microenvironmental regulation of tumor progression and metastasis. *Nat Med* **19**, 1423–1437.

[4] Lunt SJ, Chaudary N, and Hill RP (2009). The tumor microenvironment and metastatic disease. *Clin Exp Metastasis* **26**, 19–34.

[5] Nguyen DX and Massagué J (2007). Genetic determinants of cancer metastasis. *Nat Rev Genet* **8**, 341–352.

[6] Hill RP, de Jaeger K, Jang A, and Cairns R (2001). pH, hypoxia and metastasis. *Novartis Found Symp* **240**, 154–165.

[7] Rofstad EK (2000). Microenvironment-induced cancer metastasis. *Int J Radiat Biol* **76**, 589–605.

[8] Chan DA and Giaccia A (2007). Hypoxia, gene expression, and metastasis. *Cancer Metastasis Rev* **26**, 333–339.

[9] Walenta S and Mueller-Klieser W (2004). Lactate: mirror and motor of tumor malignancy. *Semin Radiat Oncol* **14**, 267–274.

[10] Hirschhaeuser F, Sattler UGA, and Mueller-Klieser W (2011). Lactate: a metabolic key player in cancer. *Cancer Res* **71**, 6921–6925.

[11] Vander Heiden MG, Cantley LC, and Thompson CB (2009). Understanding the Warburg effect: the metabolic requirements of cell proliferation. *Science* **324**, 1029–1033.

[12] Yang C, Sudderth J, Dang T, Bachoo RM, McDonald JG, and DeBerardinis RJ (2009). Glioblastoma cells require glutamate dehydrogenase to survive impairments of glucose metabolism or Akt signaling. *Cancer Res* **69**, 7986–7993.

[13] Ackerman D and Simon MC (2014). Hypoxia, lipids, and cancer: surviving the harsh tumor microenvironment. *Trends Cell Biol* **24**, 472–478.

[14] Dang CV and Semenza GL (1999). Oncogenic alterations of metabolism. *Trends Biochem Sci* **24**, 68–72.

[15] Bristow RG and Hill RP (2008). Hypoxia and metabolism. Hypoxia, DNA repair and genetic instability. *Nat Rev Cancer* **8**, 180–192.

[16] Semenza GL (2014). HIF-1 mediates metabolic responses to intratumoral hypoxia and oncogenic mutations. *J Clin Invest* **123**, 3664–3671.

[17] Gatenby RA and Gillies RJ (2004). Why do cancers have high aerobic glycolysis? *Nat Rev Cancer* **4**, 891–899.

[18] LaMonte G, Tang X, Chen JLY, Wu J, Ding CKC, Keenan MM, Sangokoya C, Kung HN, Ilkayeva O, and Boros LG, et al (2013). Acidosis induces reprogramming of cellular metabolism to mitigate oxidative stress. *Cancer Metab* **1**, 23.

[19] Ghesquière B, Wong BW, Kuchnio A, and Carmeliet P (2014). Metabolism of stromal and immune cells in health and disease. *Nature* **511**, 167–176.

[20] Rofstad EK, Tunheim SH, Mathiesen B, Graff BA, Halsør EF, Nilsen K, and Galappathi K (2002). Pulmonary and lymph node metastasis is associated with primary tumor interstitial fluid pressure in human melanoma xenografts. *Cancer Res* **62**, 661–664.

[21] Rofstad EK, Rasmussen H, Galappathi K, Mathiesen B, Nilsen K, and Graff BA (2002). Hypoxia promotes lymph node metastasis in human melanoma xenografts by up-regulating the urokinase-type plasminogen activator receptor. *Cancer Res* **62**, 1847–1853.

[22] Rofstad EK (1994). Orthotopic human melanoma xenograft model systems for studies of tumour angiogenesis, pathophysiology, treatment sensitivity and metastatic pattern. *Br J Cancer* **70**, 804–812.

[23] Rofstad EK and Måseide K (1999). Radiobiological and immunohistochemical assessment of hypoxia in human melanoma xenografts: acute and chronic hypoxia in individual tumors. *Int J Radiat Biol* **75**, 1377–1393.

[24] Rofstad EK, Galappathi K, Mathiesen B, and Ruud EB (2007). Fluctuating and diffusion-limited hypoxia in hypoxia-induced metastasis. *Clin Cancer Res* **13**, 1971–1978.

[25] Hompland T, Ellingsen C, Øvrebø KM, and Rofstad EK (2012). Interstitial fluid pressure and associated lymph node metastasis revealed in tumors by dynamic contrast-enhanced MRI. *Cancer Res* **72**, 4899–4908.

[26] Øvrebø KM, Ellingsen C, Galappathi K, and Rofstad EK (2012). Dynamic contrast-enhanced magnetic resonance imaging of the metastatic potential of melanoma xenografts. *Int J Radiat Oncol Biol Phys* **83**, e121–e127.

[27] Giskeødegård GF, Cao MD, and Bathen TF (2015). High-resolution magic-angle-spinning NMR spectroscopy of intact tissue. *Methods Mol Biol* **1277**, 37–50.

[28] Sitter B, Lundgren S, Bathen TF, Halgunset J, Fjosne HE, and Gribbestad IS (2006). Comparison of HR MAS MR spectroscopic profiles of breast cancer tissue with clinical parameters. *NMR Biomed* **19**, 30–40.

[29] Wider G and Dreier L (2006). Measuring protein concentrations by NMR spectroscopy. *J Am Chem Soc* **128**, 2571–2576.

[30] Savorani F, Tomasi G, and Engelsen SB (2010). Icoshift: a versatile tool for the rapid alignment of 1D NMR spectra. *J Magn Reson* **202**, 190–202.
[31] Wang Y, Liu X, Zhang H, Sun L, Zhou Y, Jin H, Zhang H, Zhang H, Liu J, and Guo H, et al (2014). Hypoxia-inducible lncRNA-AK058003 promotes gastric cancer metastasis by targeting γ-synuclein. *Neoplasia* **16**, 1094–1106.
[32] Rofstad EK, Ruud EBM, Mathiesen B, and Galappathi K (2010). Association between radiocurability and interstitial fluid pressure in human tumor xenografts without hypoxic tissue. *Clin Cancer Res* **16**, 936–945.
[33] Hompland T, Ellingsen C, Galappathi K, and Rofstad EK (2014). DW-MRI in assessment of the hypoxic fraction, interstitial fluid pressure, and metastatic propensity of melanoma xenografts. *BMC Cancer* **14**, 92.
[34] Rofstad EK and Mathiesen B (2010). Metastasis in melanoma xenografts is associated with tumor microvascular density rather than extent of hypoxia. *Neoplasia* **12**, 889–898.
[35] Glunde K, Jiang L, Moestue SA, and Gribbestad IS (2011). Magnetic resonance spectroscopy and imaging guidance in molecular medicine: targeting and monitoring of choline and glucose metabolism in cancer. *NMR Biomed* **24**, 673–690.
[36] Moestue SA, Dam CG, Gorad SS, Kristian A, Bofin A, Mælandsmo GM, Engebråten O, Gribbestad IS, and Bjørkøy G (2013). Metabolic biomarkers for response to PI3K inhibition in basal-like breast cancer. *Breast Cancer Res* **15**, R16.
[37] Negendank W (1992). Studies of human tumors by MRS: a review. *NMR Biomed* **5**, 303–324.
[38] Aboagye EO and Bhujwalla ZM (1999). Malignant transformation alters membrane choline phospholipid metabolism of human mammary epithelial cells. *Cancer Res* **59**, 80–84.
[39] Rofstad EK, Gaustad JV, Brurberg KG, Mathiesen B, Galappathi K, and Simonsen TG (2009). Radiocurability is associated with interstitial fluid pressure in human tumor xenografts. *Neoplasia* **11**, 1243–1251.
[40] Rofstad EK, Galappathi K, and Mathiesen BS (2014). Tumor interstitial fluid pressure – a link between tumor hypoxia, microvascular density, and lymph node metastasis. *Neoplasia* **16**, 586–594.
[41] Rofstad EK, Gaustad JV, Egeland TAM, Mathiesen B, and Galappathi K (2010). Tumors exposed to acute cyclic hypoxic stress show enhanced angiogenesis, perfusion and metastatic dissemination. *Int J Cancer* **127**, 1535–1546.
[42] Rofstad EK, Mathiesen B, and Galappathi K (2004). Increased metastatic dissemination in human melanoma xenografts after subcurative radiation treatment: radiation-induced increase in fraction of hypoxic cells and hypoxia-induced up-regulation of urokinase-type plasminogen activator receptor. *Cancer Res* **64**, 13–18.
[43] Rofstad EK, Mathiesen B, Henriksen K, Kindem K, and Galappathi K (2005). The tumor bed effect: increased metastatic dissemination from hypoxia-induced up-regulation of metastasis-promoting gene products. *Cancer Res* **65**, 2387–2396.
[44] Glunde K, Shah T, Winnard Jr PT, Raman V, Takagi T, Vesuna F, Artemov D, and Bhujwalla ZM (2008). Hypoxia regulates choline kinase expression through hypoxia-inducible factor-1α signaling in a human prostate cancer model. *Cancer Res* **68**, 172–180.
[45] Fedele TA, Galdos-Riveros AC, de Farias e Melo HJ, Magalhães A, and Maria DA (2013). Prognostic relationship of metabolic profile obtained of melanoma B16F10. *Biomed Pharmacother* **67**, 146–156.
[46] Höckel M, Schlenger K, Aral B, Mitze M, Schäffer U, and Vaupel P (1996). Association between tumor hypoxia and malignant progression in advanced cancer of the uterine cervix. *Cancer Res* **56**, 4509–4515.
[47] Brizel DM, Dodge RK, Clough RW, and Dewhirst MW (1999). Oxygenation of head and neck cancer: changes during radiotherapy and impact on treatment outcome. *Radiother Oncol* **53**, 113–117.
[48] Vaupel P and Mayer A (2007). Hypoxia in cancer: significance and impact on clinical outcome. *Cancer Metastasis Rev* **26**, 225–239.
[49] Walenta S, Wetterling M, Lehrke M, Schwickert G, Sundfør K, Rofstad EK, and Mueller-Klieser W (2000). High lactate levels predict likelihood of metastases, tumor recurrence, and restricted patient survival in human cervical cancers. *Cancer Res* **60**, 916–921.
[50] Walenta S, Salameh A, Lyng H, Evensen JF, Mitze M, Rofstad EK, and Mueller-Klieser W (1997). Correlation of high lactate levels in head and neck tumors with incidence of metastasis. *Am J Pathol* **150**, 409–415.
[51] Walenta S, Chau TV, Schroeder T, Lehr HA, Kunz-Schughart LA, Fuerst A, and Mueller-Klieser W (2003). Metabolic classification of human rectal adenocarcinomas: a novel guideline for clinical oncologists. *J Cancer Res Clin Oncol* **129**, 321–326.
[52] Ellingsen C, Walenta S, Hompland T, Mueller-Klieser W, and Rofstad EK (2013). The microenvironment of cervical carcinoma xenografts: associations with lymph node metastasis and its assessment by DCE-MRI. *Trans Oncol* **6**, 607–617.
[53] Kroeger M, Walenta S, Rofstad EK, and Mueller-Klieser W (1995). Growth rates or radiobiological hypoxia are not correlated with local metabolite content in human melanoma xenografts with similar vascular network. *Br J Cancer* **72**, 912–916.
[54] Walenta S, Snyder S, Haroon ZA, Braun RD, Amin K, Brizel D, Mueller-Klieser W, Chance B, and Dewhirst MW (2001). Tissue gradients of energy metabolites mirror oxygen tension gradients in a rat mammary carcinoma model. *Int J Radiat Oncol Biol Phys* **51**, 840–848.
[55] Schroeder T, Yuan H, Viglianti BL, Peltz C, Asopa S, Vujaskovic Z, and Dewhirst MW (2005). Spatial heterogeneity and oxygen dependence of glucose consumption in R3230Ac and fibrosarcomas of the Fischer 344 rat. *Cancer Res* **65**, 5163–5171.
[56] Yaromina A, Quennet V, Zips D, Meyer S, Shakirin G, Walenta S, Mueller-Klieser W, and Baumann M (2009). Co-localisation of hypoxia and perfusion markers with parameters of glucose metabolism in human squamous cell carcinoma (hSCC) xenografts. *Int J Radiat Biol* **85**, 972–980.
[57] Simonsen TG, Gaustad JV, Leinaas MN, and Rofstad EK (2012). Vascular abnormalities associated with acute hypoxia in human melanoma xenografts. *Radiother Oncol* **105**, 72–78.
[58] Gillies RJ, Robey I, and Gatenby RA (2008). Causes and consequences of increased glucose metabolism of cancers. *J Nucl Med* **49**, 24S–42S.
[59] Aboagye EO, Mori N, and Bhujwalla ZM (2001). Effect of malignant transformation on lactate levels of human mammary epithelial cells. *Adv Enzyme Regul* **41**, 251–260.
[60] Xu HN, Kadlececk S, Profka H, Glickson JD, Rizi R, and Li LZ (2014). Is higher lactate an indicator of tumor metastatic risk? A pilot MRS study using hyperpolarized ^{13}C-pyruvate. *Acad Radiol* **21**, 223–231.